

# Neural network model for implementation of electron–phonon scattering in nanoscale device simulations based on NEGF method

Satofumi Souma<sup>†</sup> and Matsuto Ogawa

Department of Electrical and Electronic Engineering, Kobe University, Kobe 657-8501, Japan

<sup>†</sup>email: ssouma@harbor.kobe-u.ac.jp

**Abstract**—We propose a neural network (NN) model to implement the electron–phonon scattering in quantum mechanical transport simulations based on the nonequilibrium Green’s function (NEGF) method. As a representative example of nanoscale device, we consider the nanowire field effect transistors (NWFETs), although the proposed scheme can be applied any device structures. In particular, given the spectrum of lesser and greater Green’s functions at the source and the drain edges of the channel in the absence of the electron–phonon scattering, we constructed the NN to predict the lesser and greater Green’s functions in the presence of scattering, which are used to calculate the terminal current of the device. The proposed scheme has been successfully implemented to predict the trend of current against the scattering strength with meaningful accuracy.

## I. INTRODUCTION

Aggressive scale down of MOSFET has been one of the key challenges in the technological evolution of the semiconductor industry to achieve simultaneously the lower power consumption, higher integration density, and higher operation speed [1], [2]. For instance, multigate (three dimensional) structures such as FinFETs, nanosheet FETs, and nanowire FETs are effective to reduce power consumption since their efficient gate electrostatic control of channel carriers over the thin semiconductor layer allows us to use lower supply voltage [3], [4].

The investigation and efficient design of such lower-power consumption devices have been significantly advanced using modeling and simulation studies so far. Among the various methods to simulate semiconductor devices, one of the most reliable schemes, especially for nanoscale devices, is the fully-quantum-mechanical simulation using non-equilibrium Green’s functions (NEGF) [5]. However, NEGF simulation requires repeated matrix operations and energy integrations to calculate the carrier density, which must be self-consistently calculated with Poisson’s equation. This procedure is computationally expensive, which hinders the research and development efforts.

Therefore it is important to reduce the computational time required for NEGF device simulations; for instance, by applying information-scientific approach [6], [7], [8], [9], [10], [11], [12], [13]. In Ref. [13], we have proposed a neural network (NN) based scheme to accelerate NEGF-based quantum-mechanical ballistic transport simulations for double gate

MOSFET as a representative example, where we implemented the convolutional neural network (CNN) model to train and predict the carrier density and local quantum capacitance distributions as output data for given potential distribution as input data. While this approach is useful in ballistic transport simulations, more realistic simulations require to take into account the effect of various scattering mechanisms such as electron–phonon scattering, impurity scattering, boundart roughness scattering, and so on. However, consideration of scattering mechanisms in NEGF formalism is time consuming due to the requirement of additional calculations of scattering self-energy functions, which have to be calculated self-consistently with the Green’s functions [14].

With this motivation, we present a feasibility study to reduce the computational cost required for the implementation of scattering in NEGF transport simulations by means of NN model approach. In particular we consider nanowire FETs (NWFETs) as a representative example, and we consider the electron–phonon scattering as a representative scattering mechanism. However, our proposed scheme can be valid for other device geometries and can be extended for other scattering mechanisms as far as we use NEGF method.

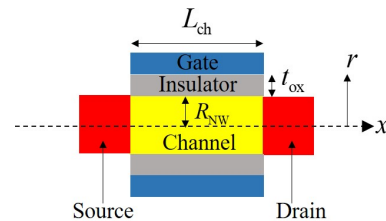


Fig. 1. Cross-sectional illustration of cylindrical gate-all-around (GAA) NWFET structure studied in this work. See text for details.

## II. MODEL AND METHOD

Figure 1 shows the cross-sectional illustration of cylindrical gate-all-around (GAA) silicon NWFET structure studied in this work, where the source and drain electrodes are doped into n-type with the doping concentration  $10^{26} \text{ m}^{-3}$ , and the gate insulator with the thickness  $t_{\text{ox}} = 1 \text{ nm}$  and the dielectric constant  $\kappa = 16$ , channel length  $L_{\text{ch}} = 10 \text{ nm}$ , and the nanowire radius  $R_{\text{NW}} = 3 \text{ nm}$ . We employ the single mode approximation and the effective mass  $m^* = 0.19m_0$  is used along the transport direction.

In NEGF device simulations central quantities are the lesser (occupied) and greater (unoccupied) Green's functions given by

$$G^{<(>)}(E) = G^R(E) \Sigma^{<(>)}(E) G^A(E), \quad (1)$$

where the lesser and the greater self-energies  $\Sigma^{<(>)}(E)$  are composed of the contact self-energy and the scattering self-energy. For instance, the self-energy  $\Sigma^<(E)$  due to the electron-phonon scattering is given within the self-consistent Born approximation as [14]

$$\begin{aligned} \Sigma_{\text{phonon}}^<(E) &= K_{\text{ac}} G^<(E) \\ &+ K_{\text{op}} \begin{bmatrix} (N_{\text{op}} + 1) G^<(E + \hbar\omega_{\text{op}}) \\ + N_{\text{op}} G^<(E - \hbar\omega_{\text{op}}) \end{bmatrix}. \end{aligned} \quad (2)$$

Here the coupling constant  $K_{\text{ac}}$  and  $K_{\text{op}}$  (with the dimension of [energy<sup>2</sup>]) can be calculated by using the deformation potential  $D_{\text{ac}}$  [energy] of acoustic phonon and the deformation field  $D_{\text{op}}$  [energy/length] of optical phonon, respectively. Here  $G^{<(>)}$  is determined through  $\Sigma^{<(>)}$  in Eq. (1), and the latter is again determined through the former in Eq. (2). Therefore  $G^{<(>)}$  is self-consistently calculated starting from those without scattering (hereafter we denote the latter as  $G_0^{<(>)}$ ), which can be calculated within less computational time in general. Once the self-consistent calculations of NEGF functions are converged, the terminal current at the left (right) contact is calculated by

$$I_{\text{L(R)}} = \frac{2e}{h} i \int dE \Gamma_{\text{L(R)}}(E) \left[ f(E - E_{\text{FL(R)}}) G_{\text{L(R)}}^>(E) + (1 - f(E - E_{\text{FL(R)}})) G_{\text{L(R)}}^<(E) \right], \quad (3)$$

where  $G_{\text{L(R)}}^{<,>}(E)$  are Green's functions at the left (right) edge of the channel, and  $f(E - E_{\text{FL(R)}})$  is the Fermi distribution function in the source (drain) electrode. This formula can be reduced to Landauer-Büttiker formula in the absence of the scattering.

Since the calculation of  $G^{<(>)}$  can be regarded as the mapping from  $G_0^{<(>)}$  (without scattering) to  $G^{<(>)}$  (with scattering), one can expect that useful NN can be constructed to generate  $G_{\text{L(R)}}^{<,>}(E)$  spectrum in the presence of scattering (output data) starting from  $G_0^{<(>)}$  spectrum (without scattering) as input data. With this observation in mind, we employ the convolutional neural network scheme, in particular, the convolutional autoencoder (encoding-decoding) scheme shown in Fig. 2, where we have four input channels ( $\text{Im}G_{\text{L0}}^<(E)$ ,  $\text{Im}G_{\text{R0}}^<(E)$ ,  $-\text{Im}G_{\text{L0}}^>(E)$ , and  $-\text{Im}G_{\text{R0}}^>(E)$ ) with  $N_{\text{ene}} = 100$  energy grid points corresponding to the input image. Scattering related parameters ( $K_{\text{ac}}$ ,  $K_{\text{op}}$ , and  $\hbar\omega_{\text{op}}$ ) are also treated as input data. We note that the scattering related parameters are injected to the encoded data of the CNN process. This is reasonable since  $G_0^{<,>}(E)$  are independent of scattering related parameters. Below we consider only the acoustic phonon scattering to demonstrate the usefulness of the proposed scheme, although the implementation of optical phonon scattering is straightforward. We consider 25 values

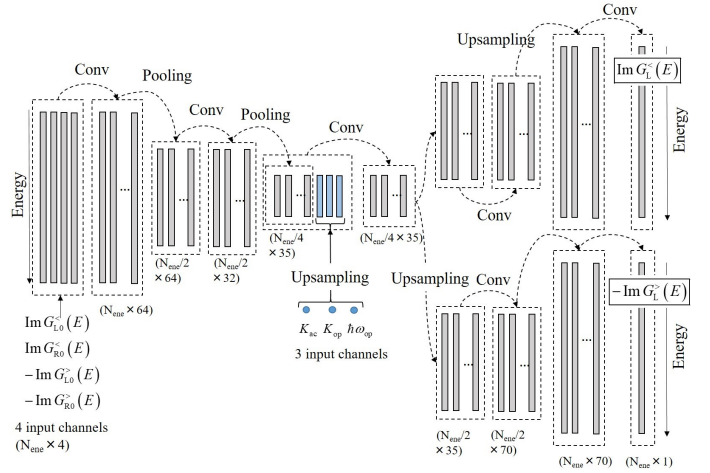


Fig. 2. Schematic illustration of the convolutional neural network model (convolutional autoencoder scheme) for the implementation of the electron-phonon scattering.

of  $V_G$  from 0 to 0.4 V and 5 values of  $\sqrt{K_{\text{ac}}}$  from 0.05 to 0.2 eV as training data.  $V_D$  is fixed at 0.3 V. Then the CNN model shown in Fig. 2 has been trained to reproduce the NEGF results. In the actual training process we have used the  $\log_{10}$  values of  $G_0^{<,>}(E)$  and  $G^{<,>}(E)$  as input and output (training) data, respectively. We note that in the present study we treat the scattering related parameters as variable input parameters to discuss the prediction ability of NN model for various electron-phonon scattering strength.

For the actual implementation we used the Keras API with the TensorFlow backend engine [15]. To fully benefit from the performance of CNN model, we use the frugally-deep library [16], which allows us to use the trained Keras models directly in our device simulator (written in C++) without requiring Python interface.

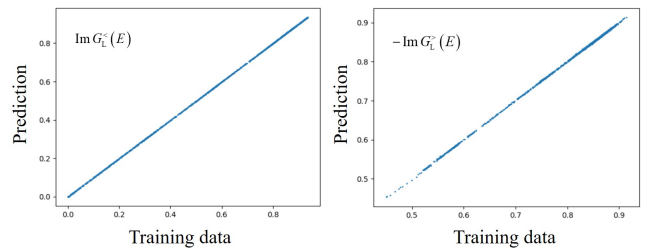


Fig. 3. Correlations between the NEGF training data (horizontal axis) and the NN predictions (vertical axis) for  $\text{Im}G_{\text{L}}^<(E)$  (left) and  $-\text{Im}G_{\text{L}}^>(E)$  (right), where the data is normalized between 0 and 1.

### III. RESULTS

In Fig. 3 we show the correlations between the NEGF training data (horizontal axis) and the NN predictions (vertical axis) for  $\text{Im}G_{\text{L}}^<(E)$  (left) and  $-\text{Im}G_{\text{L}}^>(E)$  (right), where the data is normalized between 0 and 1. As shown in this figure we have obtained good agreements between the training data and predictions.

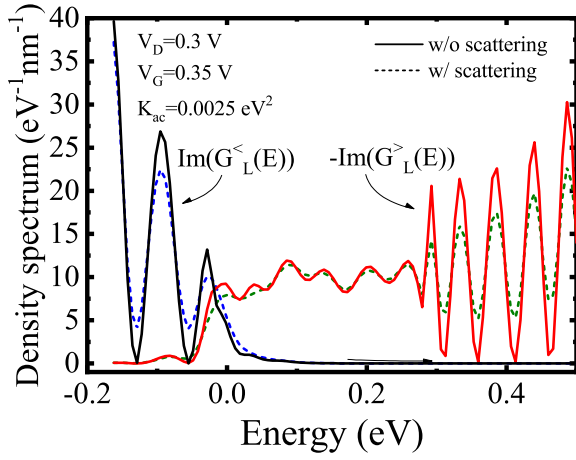


Fig. 4. Comparisons of  $\text{Im}G_L^<(E)$  and  $-\text{Im}G_L^>(E)$  between the scattering and ballistic cases. One can see the systematic relationship between them. Solid and dashed lines are the cases without and with scattering, respectively. The parameters used are  $V_D = 0.3$  V,  $V_G = 0.35$  V, and  $K_{ac}$  for scattering case is  $0.0025$   $\text{eV}^2$ .

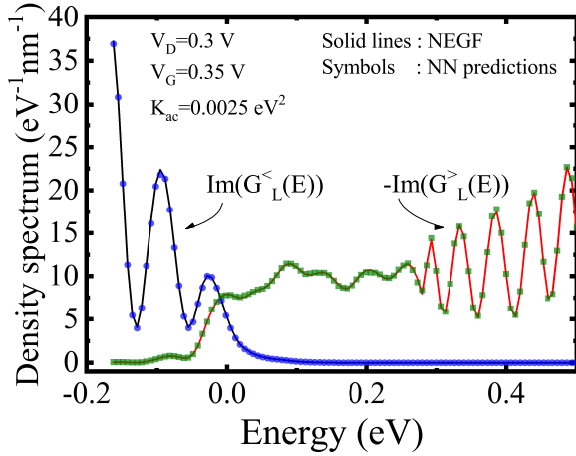


Fig. 5. Comparisons of  $\text{Im}G_L^<(E)$  and  $-\text{Im}G_L^>(E)$  between the NEGF results and the CNN predictions for the same parameters as in Fig. 4.

In Fig. 4 we show one of the specific comparisons of  $\text{Im}G_L^<(E)$  (occupation spectrum of occupied states) and  $-\text{Im}G_L^>(E)$  (occupation spectrum of unoccupied states) between the scattering and ballistic cases. The parameters used are  $V_D = 0.3$  V,  $V_G = 0.35$  V, and  $K_{ac}$  for scattering case is  $0.0025$   $\text{eV}^2$ . Here one can see the systematic relationship between them, suggesting the effectiveness of the NN model. Figure 5 shows the comparisons of  $\text{Im}G_L^<(E)$  and  $-\text{Im}G_L^>(E)$  between the NEGF results and the CNN predictions, showing the excellent agreement between them as expected from Fig. 3.

Then one can make the NN predictions of the current by using Eq. (3) along with  $G_L^<,>(E)$  predicted by CNN model straightforwardly. In Fig. 6 we plotted the drain current  $I_D$  as calculated by NEGF and NN model. Here we can

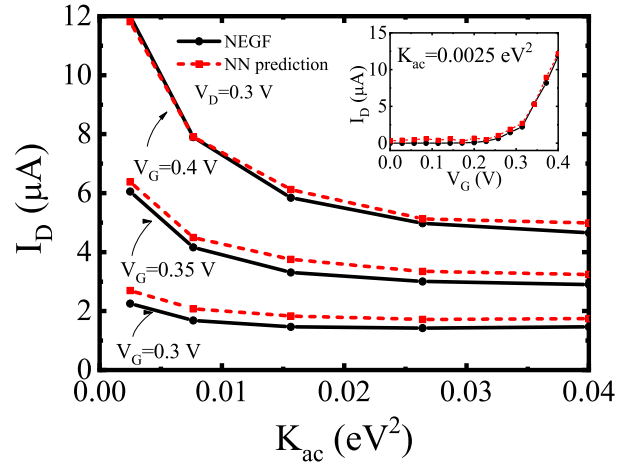


Fig. 6. The drain current  $I_D$  is plotted as a function of the acoustic phonon scattering parameter  $K_{ac}$  for three different gate voltages  $V_G$ . Results obtained by NEGF (solid lines) and NN model (dashed lines) are compared. Inset shows the  $V_G$  dependence of  $I_D$  (obtained by NEGF and NN model) for  $K_{ac} = 0.0025$   $\text{eV}^2$ .

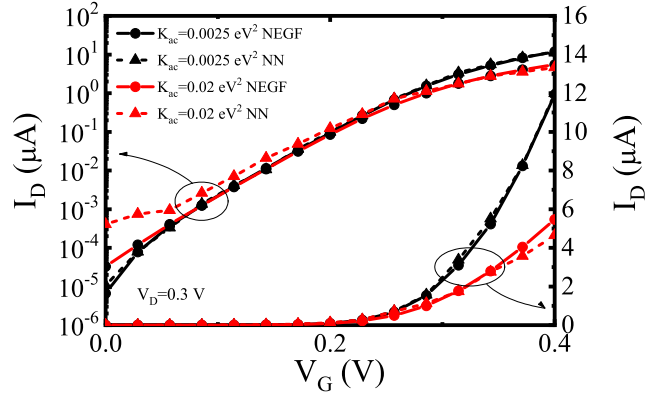


Fig. 7. Representative results of the alternative CNN scheme based on Eq. (4) (see text for detail).  $V_G$  dependence of  $I_D$  (obtained by NEGF and NN model) is shown for  $K_{ac} = 0.0025$  and  $0.2$   $\text{eV}^2$ . We note that the case  $K_{ac} = 0.0025$   $\text{eV}^2$  is included in the training data, while  $K_{ac} = 0.02$   $\text{eV}^2$  is not.

see the meaningful agreement between them. However, the discrepancy between them becomes large in the small  $V_G$  regime, and it is found that the subthreshold behavior is hardly reproduced by the above proposed scheme. This is because the magnitude of the current is determined through the 1st and the 2nd terms in Eq. (3) in a combined way, and even the extremely precise prediction of  $G_L^<,>(E)$  themselves by NN model is not enough to reproduce the subthreshold behavior accurately.

In order to overcome this difficulty, we make use of the fact

that Eq. (3) can be rewritten as

$$I_L = \frac{2e}{h} i \int dE \Gamma_L(E) f(E - E_{FL}) (1 - f(E - E_{FL})) \times i \left( \text{Im} \tilde{G}_L^<(E) + \text{Im} \tilde{G}_L^>(E) \right), \quad (4)$$

where  $\tilde{G}_L^<(E) \equiv G_L^<(E)/f(E - E_{FL})$  and  $\tilde{G}_L^>(E) \equiv G_L^>(E)/(1 - f(E - E_{FL}))$ , and their imaginary parts have the physical meaning as the effective density of states. Then we construct the similar CNN model to reproduce the function  $F(E) \equiv \text{Im} \tilde{G}_L^<(E) + \text{Im} \tilde{G}_L^>(E)$  starting from the same input data as in Fig. 2, but this time we have only one output data (i.e., the function  $F(E)$ ). We have trained this CNN model for  $F(E)$  using the same training data as before, and in Fig. 7 we show the comparison of the drain current obtained by NEGF and by the improved CNN model. As seen in Fig. 7 now we can reproduce the current with meaningful accuracy not only for the on-current regime but also in the subthreshold regime. This excellent improvement is possible because the magnitude of the current (especially in the subthreshold regime) is determined via the  $f(E - E_{FL}) (1 - f(E - E_{FL}))$  factor in Eq. (4) and remaining precise behavior is described by the function  $F(E)$  defined above, where the magnitude of the latter does not vary significantly at least within the energy range required for the current calculation, suggesting the efficient applicability of the NN model. We also note that in Fig. 7 the case  $K_{ac} = 0.0025 \text{ eV}^2$  is included in the training data, while  $K_{ac} = 0.02 \text{ eV}^2$  is not. Nevertheless the current in the case  $K_{ac} = 0.02 \text{ eV}^2$  has been successfully predicted, meaning the practical generalizability of the proposed model.

#### IV. CONCLUSION

We proposed a NN model to implement the electron-phonon scattering in quantum mechanical transport simulations based on the nonequilibrium Green's function (NEGF) method. In particular, given the spectrum of lesser and greater Green's functions at the source and the drain edges of the channel in the absence of the electron-phonon scattering, we constructed the NN to predict the lesser and greater Green's functions in the presence of scattering, which are used to calculate the terminal current of the device. We first proposed the model to predict  $G_L^<(E)$  and  $G_L^>(E)$  independently through the CNN process. This model is conceptually simple, and can predict  $G_L^<(E)$  and  $G_L^>(E)$  with enough accuracy, although it is not appropriate for the prediction of the subthreshold current behavior due to the structural feature of Eq. (3). We note that this model has another merit that it can be easily generalized to predict full  $G^{<>}$  (not only the edge components). We also proposed an alternative CNN scheme based on the different (but equivalent) expression of the current Eq. (4). This latter scheme can overcome the above mentioned difficulty in the first model, and can predict even the subthreshold current behavior with meaningful accuracy.

#### ACKNOWLEDGMENTS

This work was partially supported by JSPS KAKENHI Grant No. 19H04546.

#### REFERENCES

- [1] International Roadmap for Devices and Systems (2019) <https://irds.ieee.org/>
- [2] E. Pop: "Energy dissipation and transport in nanoscale devices," *Nano. Res.* **3** 147 (2010) 147 (DOI: 10.1007/s12274-010-1019-z).
- [3] R. S. Pal, et al.: "Recent trend of FinFET devices and its challenges: A review," 2017 Conference on Emerging Devices and Smart Systems (ICEDSS), Tiruchengode (2017) 150 (DOI: 10.1109/ICEDSS.2017.8073675).
- [4] S. Verma, et al.: "Performance analysis of FinFET device using qualitative approach for low-power applications," 2019 Devices for Integrated Circuit (DevIC), Kalyani, India (2019) 84 (DOI: 10.1109/DEVIC.2019.8783754).
- [5] S. Datta: *Electronic Transport in Mesoscopic Systems* (Cambridge University Press, UK, 1997).
- [6] F. Djeflal, et al.: "An approach based on neural computation to simulate the nanoscale CMOS circuits: application to the simulation of CMOS inverter," *Solid State Electron.* **51** (2007) 48 (DOI: 10.1016/j.sse.2006.12.004).
- [7] F. Djeflal, et al.: "A neural approach to study the scaling capability of the undoped double-gate and cylindrical gate all around MOSFETs," *Mater. Sci. Eng. B* **147** (2008) 239 (DOI: 10.1016/j.mseb.2007.08.034).
- [8] K. Tamersit and F. Djeflal: "A computationally efficient hybrid approach based on artificial neural networks and the wavelet transform for quantum simulations of graphene nanoribbon FETs," *J. Comput. Electron.* **18** (2019) 813 (DOI: 10.1007/s10825-019-01350-2).
- [9] J. Zhang, et al.: "Prior knowledge input neural network method for GFET description," *J. Comput. Electron.* **15** (2019) 911 (DOI: 10.1007/s10825-016-0842-1).
- [10] S.-C. Han and S.-M. Hong, "Deep neural network for generation of the initial electrostatic potential," *Proc. of International Conference on Simulation of Semiconductor Processes and Devices* (2019) 45 (DOI: 10.1109/SISPAD.2019.8870521).
- [11] S.-C. Han, J. Choi, and S.-M. Hong, "Electrostatic Potential Profile Generator for Two-Dimensional Semiconductor Devices," *Proc. of International Conference on Simulation of Semiconductor Processes and Devices*, 297 (2020). (DOI: 10.23919/SISPAD49475.2020.9241661).
- [12] J. Xu and D. E. Root, "Artificial neural networks for compound semiconductor device modeling and characterization," *Proc. of IEEE Compound Semiconductor Integrated Circuit Symposium (CSICS)*, (2017) (DOI: 10.1109/CSICS.2017.8240446).
- [13] S. Souma and M. Ogawa, "Acceleration of nonequilibrium Green's function simulation for nanoscale FETs by applying convolutional neural network model" *IEICE Electronics Express*, 17.20190739 (2020).
- [14] S. Souma and M. Ogawa, "Impact of electron-phonon scattering on the strain-induced current-blocking effect in graphene field-effect transistors," *Journal of Applied Physics* 127 (9), 094304 (2020).
- [15] Keras: Deep learning library for Theano and TensorFlow (2015), <https://keras.io/>
- [16] Frugally-deep library, <https://github.com/Dobiasd/frugally-deep>